Dynamic modeling of superresolution photoinduced-inhibition nanolithography

Zongsong Gan, Yaoyu Cao, Baohua Jia, and Min Gu*

Centre for Micro-Photonics and Centre for Ultrahigh-bandwidth Devices for Optical Systems (CUDOS), Faculty of Engineering and Industrial Science, Swinburne University of Technology, P.O. Box 218, Hawthorn, VIC 3122, Australia
*mgu@swin.edu.au

Abstract: A dynamical model based on the photo-physics and photo-chemistry processes for superresolution photoinduced-inhibition nanolithography (SPIN) under both single-photon and two-photon excitation is developed and validated by experimental results. Numerical simulation results for the dot fabrication predict that the theoretical single dot size can be infinitely reduced, which shows diffraction-unlimited feature of the SPIN. A small reaction constant of the inhibitor polymerization is crucial to realize a small dot size and high resolution. It is discovered both theoretically and experimentally that the dot minimum size and best resolution occur under different inhibition beam powers because of the influence from the inhibitor polymerization. Moreover, due to the consumption of the photo-inhibitor molecules in the inhibition process, the dot size may vary during the sequential fabrication.

©2012 Optical Society of America

OCIS codes: (000.4430) Numerical approximation and analysis; (140.3450) Laser-induced chemistry; (160.5470) Polymers; (220.4241) Nanostructure fabrication; (220.4610) Optical fabrication.

References and links

1. J. W. Perry, B. H. Cumpston, S. P. Ananthavel, S. Barlow, D. L. Dyer, J. E. Ehrlich, L. L. Erskine, A. A. Heikal, S. M. Kuebler, I.-Y. S. Lee, D. McCord-Maughon, J. Qin, H. Röckel, M. Rumi, X.-L. Wu, and S. R. Marder, "Two-photon polymerization initiators for three-dimensional optical data storage and microfabrication," Nature **398**(6722), 51–54 (1999).
2. M. Deubel, G. von Freymann, M. Wegener, S. Pereira, K. Busch, and C. M. Soukoulis, "Direct laser writing of three-dimensional photonic-crystal templates for telecommunications," Nat. Mater. **3**(7), 444–447 (2004).
3. S. Kawata, H. B. Sun, T. Tanaka, and K. Takada, "Finer features for functional microdevices," Nature **412**(6848), 697–698 (2001).
4. K. K. Seet, V. Mizeikis, S. Matsuo, S. Juodkazis, and H. Misawa, "Three-dimensional spiral architecture photonic crystals obtained by direct laser writing," Adv. Mater. **17**(5), 541–545 (2005).
5. M. Gu, B. Jia, J. Li, and M. J. Ventura, "Fabrication of three-dimensional photonic crystals in quantum-dot-based materials," Laser Photon. Rev. **4**(3), 414–431 (2010).
6. J. Li, B. Jia, and M. Gu, "Engineering stop gaps of inorganic-organic polymeric 3D woodpile photonic crystals with post-thermal treatment," Opt. Express **16**(24), 20073–20080 (2008).
7. M. Straub and M. Gu, "Near-infrared photonic crystals with higher-order bandgaps generated by two-photon photopolymerization," Opt. Lett. **27**(20), 1824–1826 (2002).
8. J. Serbin and M. Gu, "Experimental evidence for superprism effects in three-dimensional polymer photonic crystals," Adv. Mater. **18**(2), 221–224 (2006).
9. T. F. Scott, B. A. Kowalski, A. C. Sullivan, C. N. Bowman, and R. R. McLeod, "Two-color single-photon photoinitiation and photoinhibition for subdiffraction photolithography," Science **324**(5929), 913–917 (2009).
10. Y. Cao, Z. Gan, B. Jia, R. A. Evans, and M. Gu, "High-photosensitive resin for super-resolution direct-laser-writing based on photoinhibited polymerization," Opt. Express **19**(20), 19486–19494 (2011).
11. L. G. Lovell, B. J. Elliott, J. R. Brown, and C. N. Bowman, "The effect of wavelength on the polymerization of multi(meth)acrylates with disulfide/benzilketal combinations," Polymer (Guildf.) **42**(2), 421–429 (2001).
12. J. H. Lee, R. K. Prud'homme, and I. A. Aksay, "Cure depth in photopolymerization: experiments and theory," J. Mater. Res. **16**(12), 3536–3544 (2001).
13. N. Hayki, L. Lecamp, N. Desilles, and P. Lebaudy, "Kinetic study of photoinitiated frontal polymerization: influence of UV light intensity variations on the conversion profiles," Macromolecules **43**(1), 177–184 (2010).
14. M. R. Gleeson, S. Liu, S. O'Duill, and J. T. Sheridan, "Examination of the photoinitiation processes in photopolymer materials," J. Appl. Phys. **104**(6), 064917 (2008).

#165154 - $15.00 USD Received 21 Mar 2012; revised 1 Jul 2012; accepted 5 Jul 2012; published 11 Jul 2012

15. S. Blaya, L. Carretero, R. F. Madrigal, M. Ulibarrena, P. Acebal, and A. Fimia, “Photopolymerization model for holographic gratings formation in photopolymers,” Appl. Phys. B **77**(6-7), 639–662 (2003).
16. M. R. Gleeson and J. T. Sheridan, “Nonlocal photopolymerization kinetics including multiple termination mechanisms and dark reactions. part I. modeling,” J. Opt. Soc. Am. B **26**(9), 1736–1745 (2009).
17. W. D. Cook, “Photopolymerization kinetics of dimethacrylates using the camphorquinone amin initiator system,” Polymer (Guildf.) **33**(3), 600–609 (1992).
18. J. P. Fouassier, “Photopolymerization reactions” in *Polymer Handbook*, 4th ed., J. Brandrup, E. H. Immergut, E. A. Grulke, eds. (Wiley, 1999), p. II/169.
19. I. V. Khudyakov and N. J. Turro, “Cage effect dynamics under photolysis of photoinitiators,” Des. Monomers Polym. **13**, 487–496 (2010).
20. P. Török, P. Varga, Z. Laczik, and G. R. Booker, “Electromagnetic diffraction of light focused through a planar interface between materials of mismatched refractive index: an integral representation,” J. Opt. Soc. Am. A **12**(2), 325–332 (1995).
21. B. Chen, Z. Zhang, and J. Pu, “Tight focusing of partially coherent and circularly polarized vortex beams,” J. Opt. Soc. Am. A **26**(4), 862–869 (2009).
22. M. Gu, *Advanced Optical Imaging Theory* (Springer, 2000).
23. C. Y. Park and S. K. Ihm, “Percolation analysis on free radical linear polymerization with instantaneous initiation,” Polym. Bull. **24**(5), 539–543 (1990).
24. I. V. Khudyakov, W. S. Fox, and M. B. Purvis, “Photopolymerization of vinyl acrylate studied by photodsc,” Ind. Eng. Chem. Res. **40**(14), 3092–3097 (2001).
25. G. Odian, *Principles of Polymerization*, 4th ed. (John Wiley & Sons, Inc., 2004).

1. Introduction

Nowadays, nanofabrication has become an indispensable tool for nanoscience and nanotechnology. Among the various nanofabrication tools, photolithography is highly preferred because of its low cost, great simplicity and versatility. As one of the most successful photolithography methods, direct laser writing (DLW) has been widely applied to fabricate complex three dimensional structures on the scale of micro or nano meters for broad applications in photonics [1–8]. However, the fabrication resolution of the DLW system is fundamentally limited by the laws of diffraction (known as the Abbe's law). Therefore nano-fabrication with feature size and resolution beyond the diffraction limit presents a key challenge.

Superresolution photoinduced-inhibition nanolithography (SPIN) has received increasing attention for its potential to achieve nano-lithography with a feature size on the order of tens of nano meters, which is far beyond the diffraction limit of the DLW light [9, 10]. In this case, an improvement in the feature size and resolution can be achieved by overlapping a doughnut-shaped inhibition beam and a Gaussian-mode fabrication beam in the focal region. For a SPIN system, the Gaussian beam is used to generate the free radicals and to initiate the photo-polymerization while the doughnut beam is used to produce the inhibitor radicals and to stop the photo-polymerization in the outer ring of the doughnut beam. As a result, the photo-polymerization is confined at the centre of the focal region, which leads to a smaller feature size and resolution far beyond the diffraction limit.

Compared with the single laser beam DLW method, SPIN involves two beams, which make the photo-physical and photo-chemical reactions of the fabricated material with light much more complicated. Side reactions such as the photo-polymerization initiated by the inhibition beam may significantly influence the resolution improvement [9, 11]. This leads to great inconvenience for material development. Thus, theoretical investigation of SPIN is of great significance under such a circumstance. Though photo-polymerization has been extensively studied in theory [12–15], to the best of our knowledge, the theoretical investigation of SPIN is yet to establish.

A simplified kinetic model is developed to simulate the SPIN system based on the critical dynamic photo-physics and photo-chemistry processes of the material reacting with the two beams. The reduction in fabrication feature size and the improvement in resolution are investigated based on the model. Substantial mutual constraints between the chemical and physical reactions, which limit resolution improvement, are discussed. SPIN fabrication experiments are conducted to validate the model.

2. Theoretical model

SPIN involves laser induced photo-polymerization and photo-inhibition of the fabrication system. In the focal region, the photo-initiators and photo-inhibitors interact locally with light. In each local position of the focal region, the time dependent photo-physical and photo-chemical reactions of the photo-resin with laser beams can be described as a set of differential equations, which dominate the photo-polymerization process of the photo-resin. Due to the difference of the laser intensity in the focal region for both the fabrication and the inhibition beams, each local position has a final photo-polymerization conversion-rate, which is indicated by the percentage of the monomer polymerized in the local position. For the entire focal region, a monomer conversion-rate map can be obtained. During the washing process to remove the un-polymerized photo-resin, partially polymerized photo-resin at the local positions where the monomer conversion-rate is lower than the threshold can be washed away. The remained sufficiently polymerized material forms the designed structures.

2.1 Dynamic equations in the local position

For each local position in the focal region, the fabrication beam and the inhibition beam can drive the photo-polymerization and the photo-inhibition processes, respectively. The kinetic model presented in this work is based on the reaction processes involving photo-initiation, chain-propagation, chain-termination and photo-inhibition [16]. The following differential equations were used to describe the related photo-physical and photo-chemical processes for the photo-resin under the irradiation of the two laser beams in the focal region:

$$\frac{dP_0}{dt} = -\sigma_{\mathrm{E}} I_{\mathrm{E}} (P_0 - P_1) + \tau_1 P_1 + \tau n_1 P_1 \quad (1)$$

$$\frac{dP_1}{dt} = \sigma_{\mathrm{E}} I_{\mathrm{E}} (P_0 - P_1) - \tau_1 P_1 - \tau n_1 P_1 - k_{\mathrm{d}} P_1 + k_{\mathrm{r}} P_2^2 \quad (2)$$

$$\frac{dP_2}{dt} = 2k_{\mathrm{d}} P_1 - 2k_{\mathrm{r}} P_2^2 - k_{\mathrm{i}} P_2 M - k_{\mathrm{t}} P_3 P_2 - r_{\mathrm{t}} I_2 P_2 - r_{\mathrm{kt}} I_2 P_2 \quad (3)$$

$$\frac{dP_3}{dt} = k_{\mathrm{i}} P_2 M + r_{\mathrm{i}} I_2 M - k_{\mathrm{t}} (P_3 + P_2) P_3 - r_{\mathrm{t}} I_2 P_3 - r_{\mathrm{kt}} I_2 P_3 \quad (4)$$

$$\frac{dI_0}{dt} = -\sigma_{\mathrm{S}} I_{\mathrm{S}} (I_0 - I_1) + \tau_2 I_1 + \tau n_2 I_1 \quad (5)$$

$$\frac{dI_1}{dt} = \sigma_{\mathrm{S}} I_{\mathrm{S}} (I_0 - I_1) - \tau_2 I_1 - \tau n_2 I_1 - r_{\mathrm{d}} I_1 + r_{\mathrm{r}} I_2^2 \quad (6)$$

$$\frac{dI_2}{dt} = 2r_{\mathrm{d}} I_1 - 2r_{\mathrm{r}} I_2^2 - r_{\mathrm{i}} I_2 M - r_{\mathrm{t}} (P_3 + P_2) I_2 - r_{\mathrm{kt}} (P_3 + P_2) I_2 \quad (7)$$

$$\frac{dM}{dt} = -k_{\mathrm{p}} P_3 M \quad (8)$$

In these equations, the following conditions have been used:

1. P_0 and I_0 are the local concentrations of the photo-initiator and photo-inhibitor at the ground state; P_1 and I_1 are the local concentrations of the photo-initiator and photo-inhibitor at the excited state; P_2 and I_2 are the local concentrations of the photo-initiator and photo-inhibitor formed primary radicals, respectively; P_3 is the local concentration of the initiator propagating radicals generated from the primary

#165154 - $15.00 USD Received 21 Mar 2012; revised 1 Jul 2012; accepted 5 Jul 2012; published 11 Jul 2012
(C) 2012 OSA

radicals and from the inhibitor radicals as a side effect. M is the local concentration of monomers.

2. For the photo-initiator considered, when it is excited (one-photon excitation or two-photon excitation, with the absorption cross section σ_E), the molecule is pumped to the excited state and can form two initiator primary radicals ($2k_dP_1$, Norrish type one initiator) [17] with the rate constant of the initiator primary radicals generation, k_d (for Norrish type two initiator, one initiator generates two primary radicals, but one of the generated radicals is weak. So its contribution can be omitted and only the term k_dP_1 [18] is used for this situation. As the primary radical recombination rate is slow, the recombination term in Eq. (2) is not considered).Recombination of the initiator radicals caused by the caging effect is considered ($k_rP_2P_2$) with a recombination reaction constant of photo-initiator radicals, k_r. These initiator radicals can react with monomer to form propagating radicals with the kinetic constant rate of the initiation, k_i. The propagating radicals lead to the propagation of the chain at the rate constant, k_p, which contributes to the monomer conversion. The termination of the propagating radicals and initiator radicals is also included with the constant rate of k_t. τ_1P_1 and τn_1P_1 describing the radiation and non-radiation decay from P_1 to P_0, respectively.
3. For the photo-inhibitor, when it is excited (one-photon excitation or two-photon excitation, with the absorption cross section σ_S), the molecule can be pumped to the excited state and then dissociate to generate inhibitor radicals ($2r_dI_2$) with the rate constant of the inhibitor radical generation, r_d. Recombination of the inhibitor radicals caused by the caging effect is considered ($r_rI_2I_2$) with a recombination reaction constant of photo-inhibitor radicals, r_r. Inhibitor radicals can react with the initiator radicals ($r_{kt}I_2P_2$) and the chain radicals ($r_{kt}I_2P_3$), which inhibits the polymerization with the kinetic constant r_{kt}. As a side effect, inhibitor radicals can react with monomers and form propagating radicals (r_iI_2M) with the kinetic constant r_i, which can also initiate the chain propagation with the kinetic constant of k_p, and contribute to the monomer conversion. The terminations of the inhibitor radicals with initiator primary radicals and propagating radicals generated from the inhibitor radicals are also involved with the kinetic constant r_t. τ_2I_1 and τn_2I_1 describe the radiation and non-radiation decay from I_1 to I_0, respectively.
4. The diffusion of the photo-initiator radicals, the photo-inhibitor radicals and chain radicals are also included and synchronized with the dynamic differential equations. The following simplifications are made in the model: first, the complex inhibition processes are simplified as the reactions of inhibitor radicals with the initiator primary radicals and the propagating radicals with the kinetic constant of r_{kt}, which forms inactive molecules. Other inhibition reaction processes are not considered. Second, all of the reaction kinetic parameters, which may vary during the reaction processes, are set as averaged constant values [16].
5. The initial conditions are: concentrations of initiators, inhibitors and monomers (molar percentage): $P_0 = 0.1\%$, $I_0 = 0.1\%$ and $M = 1\text{-}P_0\text{-}I_0$, while P_0 and I_0 can be tuned. For example, if no photo-inhibitor is used, I_0 is zero. The monomer conversion-rate is defined as $1\text{-}M$. Initially, P_1, P_2, P_3, I_1, I_2 and I_3 are zeros.

2.2 Laser intensity distribution in the focal region

The equations in 2.1 determine the final monomer conversion-rate for each local position. Under the irradiation of the fabrication and inhibition beams, the photo-resin in the focal region can be polymerized according to the equations in 2.1. Under the same initial conditions with the same photo-resin exposure time, the local intensities of the fabricating and the inhibition laser beams determine a monomer conversion-rate of that local position. The monomer conversion-rate map in the focal region is a function of the local intensity of the

#165154 - $15.00 USD Received 21 Mar 2012; revised 1 Jul 2012; accepted 5 Jul 2012; published 11 Jul 2012
(C) 2012 OSA

fabrication and inhibition laser beams under this situation. If the local intensities of the fabrication and inhibition laser beams are known, the final monomer conversion-rate map can be calculated.

The focus profiles of the laser beams are calculated according to [20–22]. For the fabrication beam, a coherent and linearly polarized beam (x direction polarized) is focused by a high numerical aperture (NA) objective. The circularly polarized inhibition doughnut beam going through a planar vortex phase plate is focused with the same high NA objective. For all the focal intensity calculations, the NA of the objective is 1.4. The wavelengths for the fabrication lasers are 488 nm for single photon fabrication and 800 nm for two-photon fabrication, respectively and for the inhibition laser it is 375 nm (see Fig. 1).

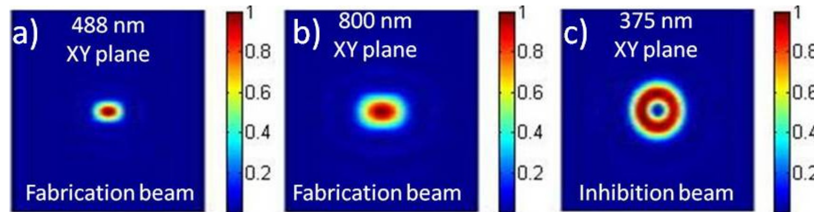

Fig. 1. Focus profiles of the fabrication laser beam with wavelengths of 488 nm (a) and 800 nm (b) for the single and two-photon excitation respectively, and inhibition beam with the wavelength of 375 nm (c) in the focal region. The calculated area is 2 μm by 2 μm.

2.3 Threshold of polymerization

Through calculating the final map of the monomer conversion-rate, the size of the fabricated structure after removing the un-polymerized part can be obtained. Generally, partially polymerized photo-resin with monomer conversion-rate lower than the threshold (gelation threshold) can be removed during the washing-out process [10]. For simulation of the dot fabrication, if the maximum monomer conversion-rate values in the final monomer conversion-rate map are lower than the threshold, all of the partially polymerized photo-resin is washed away, resulting in a zero feature size. Considering the percolation property of the polymer, the threshold of the monomer conversion-rate should be the critical point of the polymer percolation system [23]. The threshold also changes for photo-resins with different properties such as viscosity and monomer linking methods. For the same monomer conversion-rate map, the higher the threshold is, the smaller the structure size can be obtained. In this work, the threshold used is 0.33 [24].

3. Model analysis

3.1 Model validation

The model involves 18 parameters to specify the material properties. For a given material [10], the reaction constant can be fixed leaving only the laser powers of the fabrication and inhibition beams and the exposure time for the dot fabrication variable. To validate the model, a material used in our experiment is simulated. Figure 2 shows the simulation results (the initiator used here is a Norrish type two initiator) and the experiment data (details about the material, the fabrication and the washing-out process can be found in [10]).

As shown in Fig. 2, the model implies that the dot size decreases with the increase of the inhibition beam power. This prediction is confirmed by the experiment, which indicates that the model is effective and the values of the 18 parameters from the references are reliable for the material used in this work. By increasing the inhibition beam power to 5 μW, the dot size is significantly reduced from 1.23 um to 0.38 um, which means a reduction by 2/3. However, further increase of the inhibition beam power does not reduce the dot size significantly, which indicates the saturation of the inhibition effect when the inhibition beam power is high. This feature is in line with the previously reported experimental results [9].

#165154 - $15.00 USD Received 21 Mar 2012; revised 1 Jul 2012; accepted 5 Jul 2012; published 11 Jul 2012
(C) 2012 OSA

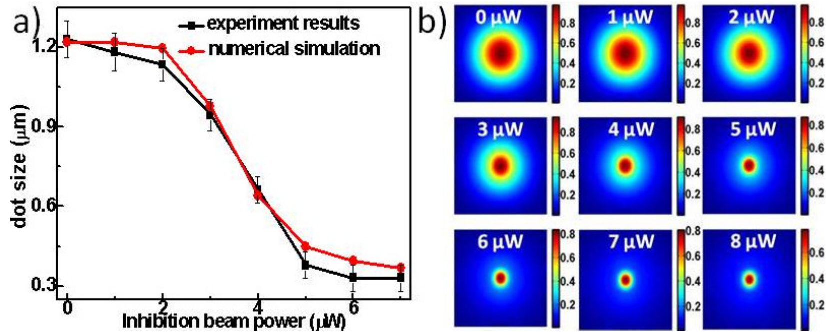

Fig. 2. (a): Dot sizes plotted as a function of the power of the inhibition laser beam. The power of the fabrication laser beam is 200 nW and the exposure time is 700 ms. The sizes of the dots in experiment were measured with a scanning electron microscope (SEM). The parameters used in the calculation are as follows: The absorption cross sections of initiators and inhibitors are 2.1×10^{-21} cm^2 and 5.9×10^{-21} cm^2, respectively; $k_d = 5 \times 10^{-5}$ s^{-1}, $r_d = 5 \times 10^{-5}$ s^{-1}; $k_i = 3 \times 10^7$ cm^{3}mol^{-1}s^{-1},$r_i = 3.6 \times 10^5$ cm^{3}mol^{-1}s^{-1}; $k_r = 1 \times 10^7$ cm^{3}mol^{-1}s^{-1}, $r_r = 1 \times 10^7$ cm^{3}mol^{-1}s^{-1}; $k_p = 2 \times 10^6$ cm^{3}mol^{-1}s^{-1}, $r_{kt} = 1.2 \times 10^8$ cm^{3}mol^{-1}s^{-1}; $k_t = 2.4 \times 10^7$ cm^{3}mol^{-1}s^{-1}, $r_t = 1.6 \times 10^7$ cm^{3}mol^{-1}s^{-1}; τ_1, τ_2, τn_1 and τn_2 are set as 1×10^2 cm^{3}mol^{-1}s^{-1}. The diffusion constant of the initiator/inhibitor radicals is 0.25μm^2/s and the diffusion constant of the chain-initiating radicals is 0.05μm^{2}s^{-1}. These values were obtained from the literatures [11, 13, 17, 19, 22, 25] and estimated from the fits to the experimental data. (b): Monomer conversion rate in the focal region at the XY plane for different levels of the inhibition beam powers. The laser beam power corresponds to the Fig. 2(a). Each of the calculated pattern area is 2 μm by 2 μm.

3.2 Photo-inhibitor induced polymerization

The function of the inhibitor radicals in the material is to inhibit the polymerization. With the polymerization at the ring region of the doughnut beam inhibited, the fabrication feature size can be tuned by the inhibition beam power. It is expected that the fabrication feature size can be infinitely reduced to approach to zero under the ideal situation. However, the inhibitor radicals have the probability to react with monomer and initiates polymerization. To make a comparison of r_i with k_i, that is the reaction constant for the initiation induced by the initiator radicals, r_i is normalized by k_i (r_i/k_i, where k_i is kept as a constant).

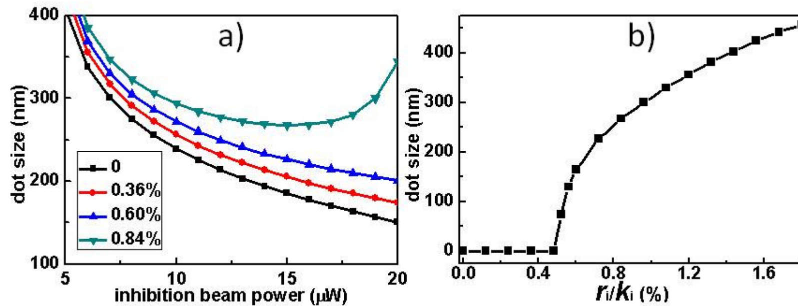

Fig. 3. (a): The dot size is plotted as a function of the inhibition laser power with different reaction constants of the inhibitor radicals with monomers (normalized by the reaction constant of the initiator radicals with monomers). (b): Calculated achievable dot minimum size for different r_i/k_i values (the inhibition laser power range is 0-121 μW; other parameters are the same as those used in Fig. 2.

As shown in Fig. 3(a), the inhibitor induced polymerization has a significant side effect on the size reduction. Dot size is increased and this phenomenon becomes more significant at high inhibition beam power, when r_i/k_i value increases. In particular, when an inhibition laser power is higher than 20 μW with r_i/k_i = 0.84%, significant photo-inhibitor induced polymerization can be observed. Under such a circumstance, there exists a minimum achievable dot size with moderate inhibition laser power. Figure 3(b) shows the minimum

#165154 - $15.00 USD Received 21 Mar 2012; revised 1 Jul 2012; accepted 5 Jul 2012; published 11 Jul 2012
(C) 2012 OSA

achievable dot size for different r_i/k_i values with the inhibition laser power ranging from 0 to 121 μW. For the situation of r_i/k_i <0.5%, the dot minimum size is zero, which means the infinitely reduced diffraction-unlimited feature size can be achieved with the SPIN in principle. For the situation of r_i/k_i >0.5%, a minimum non-zero dot size is expected. This indicates that even when the photo-inhibitor induced polymerization reaction rate is low; there exists a limitation for the minimum achievable dot size determined by the material and the fabrication parameters. For the material used in the experiment, with the same fabrication parameters as those in section 3.1, there exists a smallest dot size for different values of the inhibition beam power. But this conclusion does not mean that the smaller dot size could not be achieved with different fabrication parameters, such as a shorter exposure time. Actually, in theory, dot size infinitely approaching zero is possible if the maximum polymerization conversion rate after irradiation infinitely approaches to the threshold. However, during the washing-out process, these infinitely small structures may be washed away due to the reasons such as surface tension or weak mechanical strength. To realize infinitely small structures fabricated by the SPIN, the material is required to have small r_i value and the fabricated structures are mechanically strong to survive during the washing-out process.

3.3 Multi-dots fabrication simulation

As a candidate material for SPIN, the minimum dot size is not the only valuable data to achieve super-resolution lithography. The minimum resolvable distance between two separate dots is also valuable data for the applications such as high density data storage and photonic crystals. For the photonic crystal application, for example a woodpile structure, the smallest distance between two separate lines determines the minimum achievable lattice constants. The smallest line feature size determines the filling ratio of the woodpile with a defined lattice constant. Here, the smallest distance between two separate dots (lines) is defined as the dot (line) resolution.

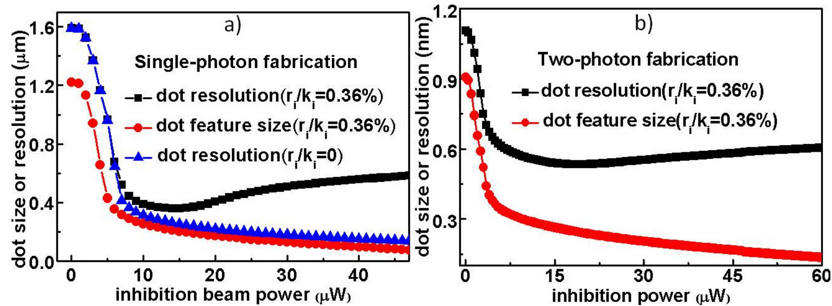

Fig. 4. Dot size and the resolution plots as a function of the inhibition laser power. For the single-photon case (a), all the parameters used are the same as those in Fig. 2. For the two-photon fabrication case (b), all the parameters related to photo-inhibitor are the same as that used in Fig. 2.

For the same parameters used in section 3.1, the dot size and the resolution are plotted as a function of the inhibition laser power as shown in Fig. 4. As is known from section 3.3, with r_i/k_i = 0.36% for the material, the fabricated dot size can be reduced to zero by increasing the inhibition beam power. However, the dot resolution does not follow the same trend as that of the dot size, which is greatly different from the single or two-photon lithography with a single beam illumination. From Fig. 4, the dot resolution can be improved by increasing the inhibition beam power. A further increasing of the inhibition beam power does not improve the dot resolution, but on the contrary deteriorate the dot resolution. For single-photon fabrication situation, the inhibition laser power to achieve the best resolution is 14μW. However, the dot size can be further reduced by increasing the inhibition beam power. In SPIN, with fixed initiation beam power, the dot minimum size and best resolution occur under different inhibition beam powers. Similar phenomenon can be observed in the two-photon fabrication case (Fig. 4(b)). Compared with the dot resolution calculation with r_i/k_i =

0 (Fig. 4(a), blue curve), we can find that this feature originates from the photo-inhibitor induced polymerization. Experiment work conducted on two-photon excitation and single-photon inhibition with the same inhibitor molecules also shows this different behavior of dot size and resolution. As shown in Fig. 5, the inhibition beam power to achieve best resolution is 4μW while the inhibition beam power to achieve smallest dot size is 7μW. This result indicates a balance between the fabrication minimum size and resolution in the SPIN for complex structure fabrication in experiment. In addition, materials with a low r_i/k_i value are vital for realizing the diffraction-unlimited property of the SPIN.

Figure 5 shows dot size and resolution for different inhibition laser powers. The dot sizes were determined from the SEM images of the separate dots. The dot resolution was determined from the shortest distance between two separate dots. From up to down, each line is eleven dot pairs fabricated with distance changing from 300 nm to 1300 nm (right to left with 100 nm increment in each step). The dot pairs fabricated with the smaller distance connect to each other and form a large dot. While the dot pairs fabricated with a distance larger than the dot resolution can be separated and remains as two dots. The smallest distance for two dots just separated is used as the experimental dot resolution. The plot in Fig. 6 shows the different dependence of the dot size and resolution on the inhibition beam power.

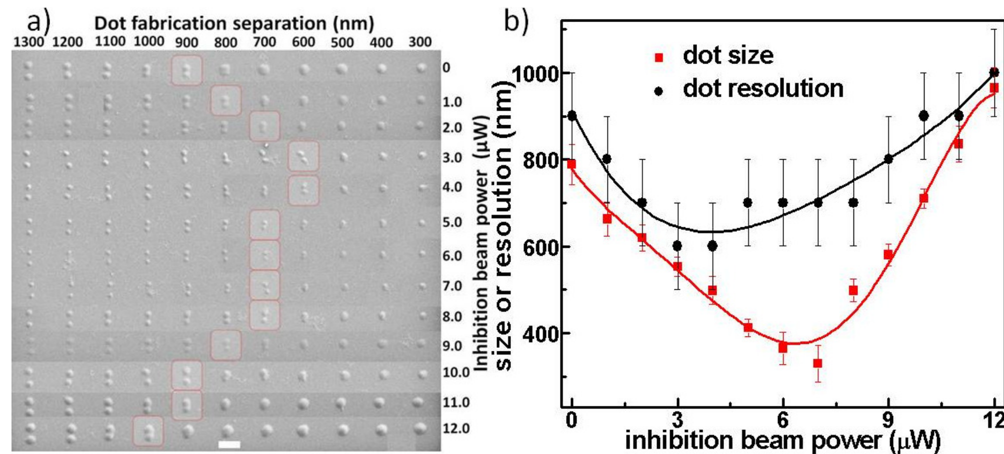

Fig. 5. The variation of the dot size and resolution with the inhibition laser power. The dots were fabricated with the fabrication beam power of 20 mW at the wavelength of 800 nm. The inhibition beam wavelength was 375 nm and the exposure time was 50 ms. (a): SEM image of the fabricated dots, the scale bar is 2 μm; (b): dot size and resolution date taken from the read box of the left SEM image. The black and red curves are the polynomial fitting of the experimental data to guide eyes. The formulation of the photoresin was composed of 0.02 wt% 2,5-bis(p-dimethylamino cinnamylidene) cyclopentanone, 0.5 wt% camphorquinone and 0.5 wt% ethyl4-(dimethylamino)benzoate as photoinitiator components, and 2.5 wt% TED as the photoinhibitor, and 96.48 wt% SR 349 (Sartomer Inc.). The fabrication beam laser operates at repetition rate of 80 MHz with a 140-femtosencond pulse width. The inhibition beam laser works at CW mode. These two beams are overlapped and introduced to an objective with numerical aperture 1.4. The dot fabrication exposure time is 50 ms. After fabrication, the gelated structure was washed out by rinsing the structure in pure isopropanol for 5 min, then in pure acetone for 2 sec and then in pure ethanol for 2 sec.

Finally, we investigate the effect of the photo-inhibitor concentration on the fabrication of complex structures. Figure 6 shows the simulation results of the sequential fabrication of four dots with a time interval of 3 folds of the dot exposure time for different levels of the inhibition laser power. With the increase of the inhibition laser power, the dot size and the resolution can be both improved. However at the high level of the inhibition laser power, the four dots after the fabrication are not uniform. This is because after the fabrication of the first and second dots, the photo-inhibitor molecules near the third and the forth dots have been partially consumed. When the third and forth dots are fabricated adjacent to the first and

#165154 - $15.00 USD Received 21 Mar 2012; revised 1 Jul 2012; accepted 5 Jul 2012; published 11 Jul 2012
(C) 2012 OSA

second dots, the reduced concentration of the photo-inhibitor molecules leads to the weak confinement of the polymerization and consequently a larger dot size.

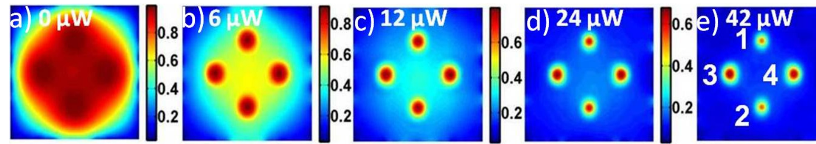

Fig. 6. Simulation of four sequentially fabricated dots for different values of the inhibition beam laser power ((a) to (e)). The first fabricated dot is plotted in the up position, the second down, the third left and the forth right. All the parameters are the same as those used in Fig. 2. Each of the calculated pattern area is 2 μm by 2 μm.

4. Conclusion

A dynamical model based on the photo-physics and the photo-chemistry processes for the single-photon and two-photon SPIN systems has been established. With this model, the dot fabrication by SPIN has been studied. Numerical simulation results indicate that SPIN can effectively reduce the dot size to nanometer resolution, which shows the diffraction-unlimited property of this technique. The reasons limiting the reduction of feature size includes the caging effect of the initiator and inhibitor radicals, single photon saturation excitation and photo-inhibitor induced polymerization. As one of the most interested and important issues for the SPIN, the photo-inhibitor induced polymerization has been investigated and the results indicate it has a significant side effect to the size reduction and resolution improvement according to the simulation. We have discovered theoretically and experimentally the dot minimum size and best resolution occur under different inhibition beam powers in the SPIN. It has been also found that the dot size in the sequential fabrication can be affected by the variation of the concentration of the photo-inhibitor molecules.

Acknowledgments

This work is produced with the assistance of the Australian Research Council (ARC) under the Centre of Excellence Program. CUDOS (the Centre for Ultrahigh-bandwidth Devices for Optical Systems) is an ARC Centre of Excellence. Min Gu thanks the Australian Research Council for its support through the Laureate Fellowship scheme (FL100100099). Baohua Jia is supported by the ARC Australian Postdoctoral Fellowship (APD) grant DP0987006.

#165154 - $15.00 USD Received 21 Mar 2012; revised 1 Jul 2012; accepted 5 Jul 2012; published 11 Jul 2012
(C) 2012 OSA